

Spin-charge conversion in disordered two-dimensional electron gases lacking inversion symmetry

Chunli Huang,^{1,2} Mirco Millettari,^{3,4} and Miguel A. Cazalilla^{5,6}

¹*Division of Physics and Applied Physics, School of Physical and Mathematical Sciences, Nanyang Technological University, Singapore 637371, Singapore*

²*Department of Physics, National Tsing Hua University, Hsinchu 30013, Taiwan*

³*Dipartimento di Matematica e Fisica, Universit Roma Tre, 00146 Rome, Italy*

⁴*Bioinformatics Institute, Agency for Science, Technology and Research (A*STAR), Singapore 138671, Singapore*

⁵*Department of Physics, National Tsing Hua University and National Center for Theoretical Sciences (NCTS), Hsinchu 30013, Taiwan*

⁶*Donostia International Physics Center (DIPC), Manuel de Lardizabal 4, 20018 San Sebastian, Spain*

(Dated: March 7, 2024)

We study the spin-charge conversion mechanisms in a two-dimensional gas of electrons moving in a smooth disorder potential by accounting for both Rashba-type and Mott's skew scattering contributions. We find that the quantum interference effects between spin-flip and skew scattering give rise to anisotropic spin precession scattering (ASP), a direct spin-charge conversion mechanism that was discovered in an earlier study of graphene decorated with adatoms [C. Huang *et al.* Phys. Rev. B **94** 085414. (2016)]. Our findings suggest that, together with other spin-charge conversion mechanisms such as the inverse galvanic effect, ASP is a fairly universal phenomenon that should be present in disordered two-dimensional systems lacking inversion symmetry.

I. INTRODUCTION

The possibility of designing spintronic devices that are entirely electrically controlled^{1,2} is attracting much attention due to the intriguing phenomena relating spin and charge transport in spin-orbit coupled (SOC) two dimensional (2D) materials and interfaces.^{3–5} Among these phenomena, the spin-Hall effect (SHE)^{3,6,7} is likely the best known example due to its close relationship to the anomalous Hall effect. In most systems exhibiting the SHE, the spin Hall conductivity receives both intrinsic and extrinsic contributions. The intrinsic contribution arises from SOC potentials respecting the translation symmetry of the crystal lattice and therefore modify the band-structure of the material. On the other hand, the extrinsic contribution originates from impurities and other kinds of disorder SOC potentials that break lattice translation symmetry and lead to momentum and spin relaxation⁸.

In addition to the SHE, systems lacking spatial inversion symmetry exhibit a closely related phenomenon, namely the current-induced spin polarization (CISP), also known as the inverse spin galvanic effect^{9–15}. Similar to the SHE, CISP can arise from both intrinsic and extrinsic mechanisms. The intrinsic mechanism was studied many systems such as semiconductor quantum wells with uniform Rashba SOC⁵ and graphene proximity to transition metal dichalcogenide¹⁶. For a 2D electron gas such as doped graphene decorated with adatoms^{17–22}, the extrinsic mechanisms were described in a recent study by some of the present authors²⁰. There, a novel scattering mechanism termed anisotropic spin precession scattering (ASP) was reported and found to yield a sizable contribution to the CISP²⁰. More recently, ASP has also been shown to give rise to an anomalous nonlocal re-

sistance in Hall bar devices²³. ASP is a form of *direct* magneto-electric effect, which arises as a quantum interference effect when an electron scatters off a single impurity that locally induces SOC by proximity. Physically, it corresponds to a polarization of the electron spin caused by scattering with the impurities. The existence of ASP scattering requires the impurity potential to break spatial inversion, which in a 2D system means that the fluctuating electric field giving rise to the SOC potential has components both in and out of the plane of the system (cf. Fig.1a). Indeed, this condition is expected to be fulfilled in most disordered systems lacking spatial inversion symmetry. Yet, for reasons unknown to us, disorder effects that break inversion symmetry have been largely ignored when discussing the spin-charge conversion mechanisms. Note that the effect of Rashba SOC and disorder has also been discussed intensively in the broader context of spintronics in superconductors, see Ref.24–27.

In graphene decorated with adatoms,^{20,28} charge carriers can undergo resonant scattering with localized impurities,²⁰ which enhances the SHE even in the dilute impurity limit^{19,21,22}. However, in many 2D systems disorder is not well described by a superposition of well-localized impurity potentials. A well-known example is 2D electron gas (2DEG) in a semiconducting quantum well. In 2DEG, electrons experience a smooth disorder potential landscape arising from distant dopant impurities²⁹, for which defining impurity density may be difficult. Another example includes heterostructures made by placing doped graphene on a substrate such as a transition metal dichalcogenide^{30,31}. Even if the substrate is brought into close contact with graphene (in order to maximize the proximity-induced SOC), due to ripples^{32,33}, crystal lattice mismatch as well as misalignments, substrate defects and impurities, the resulting SOC potential – albeit

smooth – is expected to exhibit spatial fluctuations and lack spatial inversion symmetry.

In the case of 2DEG in quantum wells, the disorder potential results from an inhomogeneous distribution of dopant ions in the doping layer, which are typically located at a distance much larger than the atomic scale ($\sim 10\text{nm}$ of separation,³⁴ see Fig. 1a). The spatial gradient of the smooth disorder potential leads to a fluctuating electric field, which in turn gives rise to a disorder SOC potential.²⁹ The electric field has two components, one *parallel* to the plane of the 2DEG, which gives rise to a SOC that conserves the spin-projection on the axis perpendicular to the plane and leads to Mott skew scattering. The other component of the electric field is *perpendicular* to the plane of the 2DEG and will generically break the spatial inversion symmetry (i.e. $z \rightarrow -z$). This component of the electric field gives rise to spin-flip scattering mediated by Rashba SOC^{29,35–37}. Previous theoretical treatments of spin transport in the 2DEG have focused on either the Rashba-type contribution to the SOC potential^{3,8,10,38,39} or the Mott’s skew-scattering^{29,35–37}. However, in this article, we shall develop a theory of spin transport in the 2DEG that treats both disorder-induced spin-flip scattering and skew scattering on equal footing. As we argue below, this is indeed necessary in order to provide a comprehensive description of the extrinsic spin-charge conversion mechanisms. We identify various spin-charge conversion mechanisms due to quantum mechanical interference between the different contributions of the SOC disorder potential. In particular, quantum interference between the perpendicular and the parallel component of the disorder potential is shown to give rise to ASP scattering²⁰. Our findings suggest that such disorder induced, quantum interference effects should be ubiquitous in any disordered 2D material lacking spatial inversion symmetry.

The rest of the article is organized as follows: In Sec. II, we introduce the microscopic model and discuss its relationship with previously studied models. In Sec. III, we discuss the derivation of the quantum Boltzmann equation within the SU(2) Schwinger-Keldysh formalism introduced in Refs. 38–40 and the approximations used to obtain the collision integrals. The resulting linear response relationships are discussed in Sec. IV. The physical consequences of our findings are discussed in Sec. V, with emphasis on the current-induced spin-polarization and the spin Hall effect. Then in Sec. VI, we provide some estimation of our main results using the experiment data from Ref. 41. Finally, we close the article with a summary. Technical details concerning the derivation of the quantum Boltzmann equation are presented in the appendix.

II. MICROSCOPIC MODEL

The Hamiltonian of the model studied below can be written as

$$H = \frac{(\mathbf{p} + \sum_a \mathcal{A}^a \sigma^a / 2)^2}{2m} + U(\mathbf{r}), \quad (1)$$

where $\mathbf{p} = (p_x, p_y)$ (momentum) and $\mathbf{r} = (x, y)$ (position) are two dimensional vectors lying in the XY plane (i.e. $z = 0$) to which the 2DEG is confined. The Pauli matrices σ^a ($a = x, y, z$) describe the electron spin. \mathcal{A} is the non-abelian gauge field describing the uniform SOC; in our model, its non-vanishing components are $\mathcal{A}_x^y = -\mathcal{A}_y^x = -2m\alpha$ where α is the potential strength of the uniform Rashba SOC. The upper and lower indices refer to the spin and orbital degree of freedom, respectively. In this article, we shall use units where $\hbar = e = 1$.

We assume the electrons move in a random disorder potential, $U(\mathbf{r})$, which is generated by e.g. the dopants in the quantum well²⁹. Generically, besides a spin-independent potential, $U(\mathbf{r})$ contains a SOC potential, which consists of a term accounting for Mott scattering^{3,8,38} and a Rashba-type potential^{29,35–37}. Mathematically,

$$U(\mathbf{r}) = V(\mathbf{r}, 0) - \frac{\lambda_{\parallel}^2}{4} (\mathbf{p} \times \nabla V(\mathbf{r}, 0)) \cdot \boldsymbol{\sigma} + \frac{\lambda_{\perp}^2}{8} (\sigma_x \{p_y, \partial_z V(\mathbf{r}, 0)\} - \sigma_y \{p_x, \partial_z V(\mathbf{r}, 0)\}). \quad (2)$$

Here $V(\mathbf{r}, z)$ is the fluctuating electric potential created (in the three dimensional region of the material that contains the 2DEG) by the dopant impurities; λ_{\parallel} and λ_{\perp} are the (material dependent) effective Compton-wavelengths. The second (third) term on the right hand side of Eq. (2) stems for the component of the electric field parallel (perpendicular) to the XY plane and corresponds to the Mott (Rashba) potential. The breaking of spatial inversion symmetry from disorder effects are described by the Rashba disorder potential (i.e. last term in Eq. (2)). The effect of this term on the carrier spin relaxation was studied in Refs. 29, 35–37. For a smooth disorder potential, we can take $\partial_z V(\mathbf{r}, 0) \simeq V(\mathbf{r}, 0)/\xi + g(\mathbf{r})$, where ξ is the transverse confinement length of the 2DEG. Here $g(\mathbf{r})$ represents the component of the perpendicular electric field that is uncorrelated to the in the plane potential, i.e. $\langle g(\mathbf{r})V(\mathbf{r}, 0) \rangle = 0$, see e.g. the supplementary Materials of Ref. 41. Note that $g(\mathbf{r})$ shifts the Elliott-Yafet relaxation time but it does not induce any spin-charge coupling since $\langle g(\mathbf{r})V(\mathbf{r}, 0) \rangle = 0$. Therefore, to the leading order in $V(\mathbf{r}, 0)/(g(\mathbf{r})\xi) \gg 1$, the matrix elements of the disorder potential in the plane-wave basis can be evaluated to yield

$$\langle \mathbf{k} | U | \mathbf{p} \rangle = V_{\mathbf{k}\mathbf{p}} \left[1 - i \lambda_z \Gamma_M(\hat{\mathbf{k}}, \hat{\mathbf{p}}) - \lambda_{xy} \Gamma_R(\hat{\mathbf{k}} + \hat{\mathbf{p}}) \right], \quad (3)$$

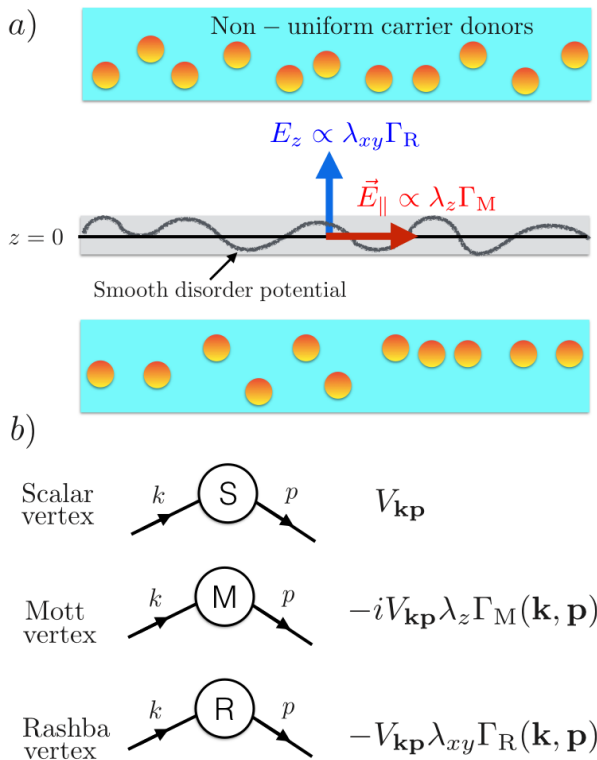


FIG. 1. a) The dopants in the quantum well create a smooth disorder landscape upon which the carriers in the two-dimensional electron gas move. The perpendicular (parallel) component of the electric field gives rise to a SOC potential of the Rashba (Mott) type. b) The Feynman diagrams for the self-energy are obtained from three types of scattering vertices describing the scattering events with the spin orbit coupling disorder potential. The vertices are the spin-independent scalar vertex, the Mott scattering vertex $\Gamma_M(\mathbf{k}, \hat{\mathbf{p}}) = (\mathbf{k} \times \hat{\mathbf{p}}) \cdot \boldsymbol{\sigma}$ which conserves spin in the z -direction and the Rashba SOC vertex $\Gamma_R(\hat{\mathbf{p}}) = (\boldsymbol{\sigma} \times \hat{\mathbf{p}}) \cdot \hat{\mathbf{z}}$ which does not conserve in the z -direction.

where $\hat{\mathbf{k}} = \mathbf{k}/k$, and $\hat{\mathbf{p}} = \mathbf{p}/p$ and

$$V_{\mathbf{k}\mathbf{p}} = V_{\mathbf{k}-\mathbf{p}} = \frac{1}{A} \int d\mathbf{r} e^{i(\mathbf{p}-\mathbf{k}) \cdot \mathbf{r}} V(\mathbf{r}, 0) \quad (4)$$

is the Fourier transform of the in-plane disorder electric potential. From here and what follows, we set the area of the 2D electron gas $A = 1$. $\Gamma_M(\hat{\mathbf{k}}, \hat{\mathbf{p}}) = (\hat{\mathbf{k}} \times \hat{\mathbf{p}}) \cdot \boldsymbol{\sigma}$ and $\Gamma_R(\hat{\mathbf{p}}) = (\boldsymbol{\sigma} \times \hat{\mathbf{p}}) \cdot \hat{\mathbf{z}}$ are the interaction vertices for the Mott and Rashba scattering respectively. The dimensionless vertex strength λ_{xy} and λ_z can be treated as phenomenological parameters that parametrize the theory in different disorder regimes. For our microscopic model (at zero temperature), these parameters take the following values: $\lambda_{xy} = p_F \lambda_{\perp}^2 / 8\xi$ and $\lambda_z = p_F^2 \lambda_{\parallel}^2 / 4$, where p_F is the Fermi momentum. In order to capture skew scattering and quantum interference effects one needs to go beyond the Gaussian approximation^{21,22} and consider up to the third moment in the distribution of the random

potential:

$$\langle V_{\mathbf{p}} \rangle = 0 \quad (5)$$

$$\langle V_{\mathbf{p}} V_{\mathbf{q}} \rangle = n_s v_0^2 \delta(\mathbf{p} + \mathbf{q}), \quad (6)$$

$$\langle V_{\mathbf{p}} V_{\mathbf{q}} V_{\mathbf{k}} \rangle = n_s v_0^3 \delta(\mathbf{p} + \mathbf{q} + \mathbf{k}). \quad (7)$$

Here, v_0 is the strength of the impurity potential while n_s has dimension of inverse area and it is usually identified with the impurity density. However, since in our model the electrons are scattered by a random – albeit smooth – potential, it is difficult to clearly identify n_s as an impurity density. In what follows, n_s should be understood as parametrizing the smoothness of the disorder landscape, depending itself on microscopic parameters such as the density of donors, the distance between the doping layer and the 2DEG, and the Thomas-Fermi screening length²⁹.

III. QUANTUM BOLTZMANN EQUATION

In this section we obtain the quantum Boltzmann equation describing coherent spin transport by means of the SU(2) Schwinger-Keldysh formalism developed in Refs. 38 and 39 [see also the appendix A for details]. Under the influence of an electric (\mathbf{E}) and magnetic field (\mathcal{H}^a), the (matrix) distribution function $n_{\mathbf{p}}(\mathbf{r}, t)$ satisfies the following equation:

$$\left(\nabla_t n_{\mathbf{p}} + \frac{\mathbf{p}}{m} \cdot \nabla_{\mathbf{r}} n_{\mathbf{p}} \right) + \frac{1}{2} \{ \mathbf{F}_{\mathbf{p}}, \partial_{\mathbf{p}} n_{\mathbf{p}} \} = I[n_{\mathbf{p}}]. \quad (8)$$

Here $\mathbf{F}_{\mathbf{p}} = \mathbf{E} + \frac{\mathbf{p}}{m} \times \boldsymbol{\mathcal{B}}$ is the force acting on the electrons moving with velocity \mathbf{p}/m , and $\boldsymbol{\mathcal{B}} = 8m^2 \alpha^2 \hat{\mathbf{z}} \sigma^z$ is the effective ‘‘magnetic field’’ induced by the uniform Rashba SOC; $\nabla_{\mathbf{r}}$ and ∇_t are covariant derivatives accounting for spin precession induced by the SOC and the magnetic fields^{38,39}:

$$\nabla_t n_{\mathbf{p}}(\mathbf{r}, t) = \partial_t n(\mathbf{p}, \mathbf{r}, t) - i[(-\gamma \mathcal{H}^a \sigma^a), n_{\mathbf{p}}(\mathbf{r}, t)], \quad (9)$$

$$\nabla_{\mathbf{r}} n_{\mathbf{p}}(\mathbf{r}, t) = \partial_{\mathbf{r}} n(\mathbf{p}, \mathbf{r}, t) + i[\boldsymbol{\mathcal{A}}^a \sigma^a, n_{\mathbf{p}}(\mathbf{r}, t)], \quad (10)$$

where γ is the gyromagnetic ratio. The left hand side of Eq. (8) describes the drift and diffusion of spin and charge due to both the uniform SOC and the external field. The right hand-side of Eq. (8) is the so-called collision integral. We assume that the disorder induced, spin-orbit coupling strength is weak ($\lambda_{xy} \sim \lambda_z \ll 1$) and therefore omit terms that are proportional to third and higher order in λ_{xy}, λ_z , and $v_0^3 \lambda_{xy}, v_0^3 \lambda_z$. In the standard, semiclassical Boltzmann equation, $I[n_{\mathbf{p}}]$ is assumed to be independent⁴² of \mathbf{E} . However, this assumption neglects quantum interference effects between the electric field and the SOC potential. The side-jump contribution to spin-Hall effect precisely arises as a quantum mechanical correction to the velocity operator⁸ \mathbf{p}/m . For these reasons, terms in the collision integral $I[n_{\mathbf{p}}]$ up to linear order in the components of electric field E_{λ_z} and $E_{\lambda_{xy}}$

must be retained. Furthermore, in the derivation of the right hand-side of Eq. (8), we assumed a weak *uniform* SOC strength, that is, $\alpha \ll v_F$, where $v_F = p_F/m$ is the Fermi velocity. Therefore, we neglect any corrections to $I[n_{\mathbf{p}}]$ arising from the uniform SOC potential (α or \mathcal{A}). Within the above approximations, we find that the collision integral can be associated with *seven* distinct classes of self-energy diagrams shown in Fig. 2. In the absence of an external magnetic field (i.e. for $\mathcal{H} = 0$), and for a uniform external electric field \mathbf{E} , the quantum Boltzmann equation in the steady state takes the form:

$$\begin{aligned} & i[e\mathcal{A}\sigma^a \cdot \frac{\mathbf{p}}{m}, n_{\mathbf{p}}] + \frac{1}{2} \{e\mathbf{E} + \mathbf{p} \times (\hat{\mathbf{z}}\omega_c\sigma^z), \partial_{\mathbf{p}}n_{\mathbf{p}}\} \\ & = I_{\text{D}}[n_{\mathbf{p}}] + I_{\text{EY}}[n_{\mathbf{p}}] + I_{\text{RS}}[n_{\mathbf{p}}] + I_{\text{SS}}[n_{\mathbf{p}}] + I_{\text{SJ}}[n_{\mathbf{p}}] \\ & \quad + I_{\text{ASP}}[n_{\mathbf{p}}]. \end{aligned} \quad (11)$$

Note that the covariant space derivative does not vanish even for the uniform steady state where $n_{\mathbf{p}}$ is independent of \mathbf{r} but contributes a spin-precession term induced by the uniform SOC³⁸. Here we have parametrized the strength of the effective SOC magnetic field using $\omega_c = |\mathcal{B}|/m = 8m\alpha^2$, which is the cyclotron frequency induced by the uniform SOC. The collision integrals on the right hand side of Eq. (11) correspond respectively to: Drude relaxation, Elliott-Yafet relaxation, Rashba Scattering, skew scattering, side-jump and anisotropic spin precession scattering. Their evaluation is described in Appendix B.

IV. LINEAR RESPONSE MATRIX

As discussed in e.g. Refs. 20 and 43, in the steady state the quantum Boltzmann equation can be solved using the following *ansatz*:

$$n_{\mathbf{p}} = n_{\text{FD}}[\epsilon_p - \mathbf{p} \cdot \mathbf{v}_c - ((\mathbf{p} \cdot \mathbf{v}_s) \hat{\mathbf{n}}_1 + h_0 \hat{\mathbf{n}}_0) \cdot \boldsymbol{\sigma}]. \quad (12)$$

Here $n_{\text{FD}}(\epsilon) = [e^{(\epsilon-\mu)/kT} + 1]^{-1}$ is the Fermi-Dirac distribution function, $\epsilon_p = p^2/2m$ the electron kinetic energy, \mathbf{v}_c (\mathbf{v}_s) the drift velocity of the charge (spin) degrees of freedom, h_0 is proportional to the magnitude of the magnetization, and $\hat{\mathbf{n}}_0$ and $\hat{\mathbf{n}}_1$ are respectively the directions of the magnetization and the spin current. Our ansatz amounts to solving the Boltzmann equation with an expansion in circular harmonics of the Fermi surface deformation⁴⁴. We are interested in evaluating the non-equilibrium spin polarization $\mathbf{M} = (M^x, M^y, M^z)$, the charge current density $\mathbf{J} = (J_x, J_y)$ and the spin current density $\mathcal{J}^a = (\mathcal{J}_x^a, \mathcal{J}_y^a)$ ($a = x, y, z$ is the spin orientation). At zero temperature, these observables are related

to the parameters of the *ansatz* (12) as follows:

$$M^a = \frac{1}{2} \sum_{\mathbf{p}} \text{Tr}[\sigma^a n_{\mathbf{p}}] = N_0 h_0 \hat{n}_0^a, \quad (13)$$

$$J_i = \frac{1}{2} \sum_{\mathbf{p}} \text{Tr}\left[\frac{p_i}{m} n_{\mathbf{p}}\right] = N_0 \epsilon_F \frac{(v_c)_i}{2}, \quad (14)$$

$$\mathcal{J}_i^a = \frac{1}{2} \sum_{\mathbf{p}} \text{Tr}\left[\sigma^a \frac{p_i}{m} n_{\mathbf{p}}\right] = N_0 \epsilon_F \frac{(v_s)_i \hat{n}_1^a}{2}, \quad (15)$$

where $N_0 = \sum_p \delta(\epsilon_p - \mu) = m/2\pi$ is the density of states of the 2DEG. In order to make contact with the results of Ref. 20, we shall measure the spin and charge currents in the same units and we rescale the magnetization by defining $\mathcal{M} = v_F \mathbf{M}$. Substituting Eq. (12) into Eq. (11) and setting $\mathbf{E} = E_x \hat{\mathbf{x}}$, we finally obtain the following linear response relations:

$$\begin{pmatrix} J_x \\ \mathcal{J}_y^z \\ \mathcal{M}^y \end{pmatrix} = \begin{pmatrix} 0 & \theta_{\text{SH}} & \tau_{\text{D}}\alpha_{\text{asp}} \\ -\theta_{\text{SH}} & 0 & \tau_{\text{D}}\alpha_{\text{R}} \\ \tau_{\text{EY}}^y\alpha_{\text{asp}} & -\tau_{\text{EY}}^y\alpha_{\text{R}} & 0 \end{pmatrix} \begin{pmatrix} J_x \\ \mathcal{J}_y^z \\ \mathcal{M}^y \end{pmatrix} + \begin{pmatrix} \sigma_{\text{D}} E_x \\ \sigma_{yx}^{SJ} E_x \\ 0 \end{pmatrix}. \quad (16)$$

It is easy to see that under the influence of an electric field \mathbf{E} , the 2DEG responds in three different ways: a longitudinal charge current $\mathbf{J} = J_x \hat{\mathbf{x}}$ and a transverse spin current $\mathcal{J}^z = \mathcal{J}_y^z \hat{\mathbf{y}}$ and a non-equilibrium spin-polarization $\mathcal{M} = \mathcal{M}^y \hat{\mathbf{y}}$. The direction of flow and spin-polarization of these responses is determined by the direction of the external electric field \mathbf{E} and the symmetry of the system.

The first term on the right hand side of Eq. (16) describes the coupling between responses (induced by both intrinsic and extrinsic SOC) while the second term describes their relation to the applied driving field; this is in turn characterized by the Drude conductivity σ_{D} and the contribution of the spin-Hall conductivity arising from the side-jump mechanism, σ_{yx}^{SJ} :

$$\sigma_{\text{D}} = \frac{n\tau}{m}, \quad \sigma_{yx}^{SJ} = n\lambda_s, \quad (17)$$

where $n = \sum_p f_{\text{FD}}(\epsilon_p)$ is the electron density. Most importantly, the coupling matrix in Eq. (16) is characterized by three ‘‘conversion rates’’ between different responses (i.e. $\{J_x, \mathcal{J}_y^z, \mathcal{M}^y\}$) and by two relaxation rates. The two relaxation rates are the elastic (Drude) scattering rate and the Elliott-Yafet spin scattering rate. The elastic (Drude) scattering rate and the (anisotropic) Elliott-Yafet scattering rate are given by:

$$\frac{1}{\tau_{\text{D}}} = 2\pi n_s v_0^2 N_0, \quad \frac{1}{\tau_{\text{EY}}^z} = \frac{4\lambda_{xy}^2}{\tau_{\text{D}}} \quad (18)$$

$$\frac{1}{\tau_{\text{EY}}^x} = \frac{1}{\tau_{\text{EY}}^y} = \frac{(6\lambda_{xy}^2 + \lambda_z^2)}{\tau_{\text{D}}}. \quad (19)$$

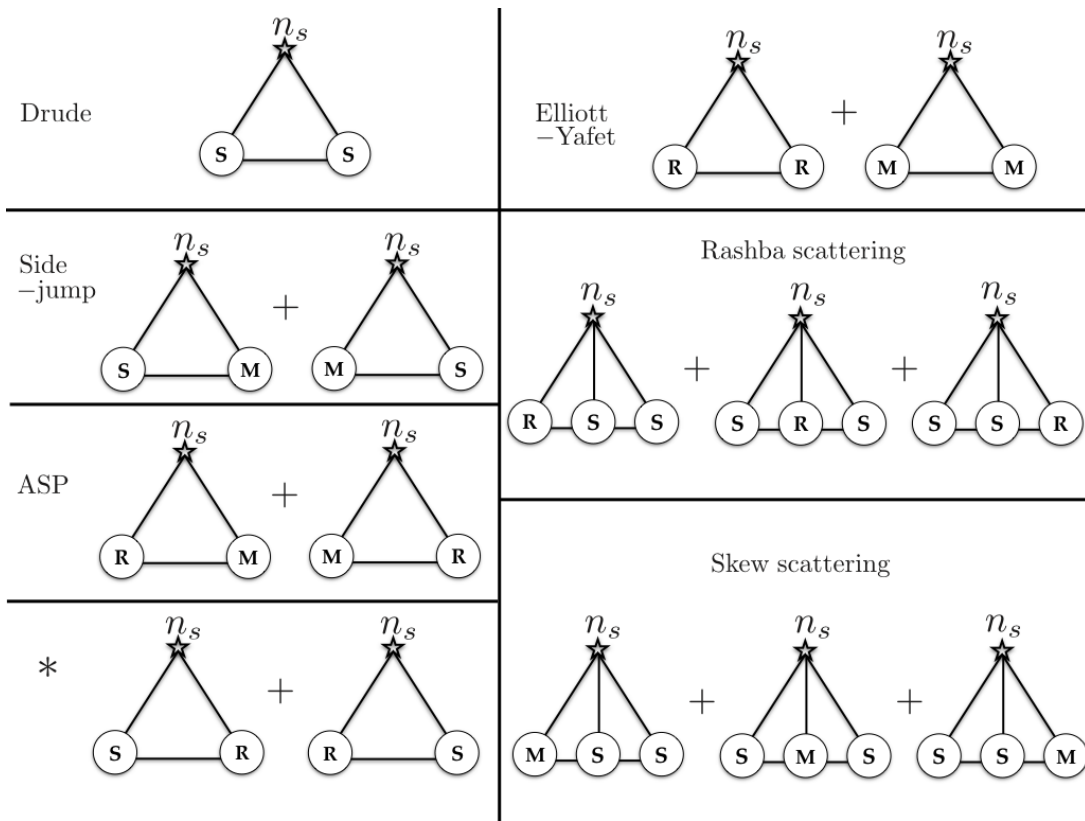


FIG. 2. Self-energy diagrams used in the evaluation of the collision integrals. The self-energy diagrams consist of three types of vertices: S, M, R. Note that the diagrams that contain different vertices lead to intriguing spin-charge conversion mechanism. In this sense, the conversion between spin and charge results from quantum interference between different components of the spin-orbit coupling potentials. Neglecting diagrams containing the Γ_R vertex, we recover the results of Ref. 38 and 39. Note that the * diagram vanishes for a non-polarized spin fermi liquid.

The other three conversion rates (or ratios) are

$$\alpha_R = p_F (\alpha + \delta\alpha_R), \quad (20)$$

$$\alpha_{\text{asp}} = -4 \lambda_{xy} \lambda_z \tau_D^{-1}, \quad (21)$$

$$\theta_{\text{SH}} = 2\pi v_0 N_0 \lambda_z + \omega_c \tau_D. \quad (22)$$

α_R is the conversion rate between the (macroscopic) spin-current \mathcal{J}_y^z and the non-equilibrium magnetization \mathcal{M}^y . In addition to the usual contribution from the uniform Rashba SOC (i.e. αp_F), it also receives a renormalization coming from the disorder induced energy shift $\delta\alpha_R$. Diagrammatically, $\delta\alpha_R$ arises from the (third order Born approximation) Rashba scattering diagram and part of the ASP diagram in Fig. 2, see Appendix B for more information. This impurity induced precession was also found in Ref. 20 as a result of self-energy correction (i.e. the part of the collision integral that is linear order in the T -matrix). Similarly, α_{asp} in Eq. (21) is the anisotropic spin precession scattering rate, inducing conversion between the (macroscopic) charge current J_x and the magnetization \mathcal{M}^y , see Fig. 2. The spin Hall angle – Eq. (22) – contains both the skew scattering and intrinsic contribution³⁸. The latter arises from the uniform Rashba SOC and is proportional to the “cyclotron fre-

quency” $\omega_c = 8m\alpha^2$. The intrinsic and skew scattering contributions arise from the non-equilibrium part of the distribution function $n_{\mathbf{p}}$. However, the side-jump contribution to the spin-Hall conductivity involves the equilibrium distribution. The difference is reflected in Eq. (16): The side-jump couples the spin current \mathcal{J}_y^z directly to the *electric field* via σ_{yx}^{SJ} . On the other hand, the intrinsic and skew scattering mechanisms couple \mathcal{J}_y^z to the *charge current*. Nevertheless, this distinction is not important when solving (16) for the total spin Hall conductivity. Note that the uniform SOC (i.e. non-abelian gauge field α) will only quantitatively change the spin Hall angle θ_{SH} and the Rashba conversion rate α_R , but it will leave the form of the linear response equation (Eq. 16) unchanged.

The linear response matrix, Eq. (16), has been obtained within the SU(2) Schwinger-Keldysh formalism assuming a weak (but smooth) disorder potential. An almost identical result has been also obtained within the Kohn-Luttinger formalism developed in Ref. 20, under the assumption that the impurity density is small (but for arbitrarily strong single-impurity potential). Notice that in the Kohn-Luttinger approach, the side-jump contribution is absent to leading order in the impurity density²⁰. However, the strong similarities between the transport

theories resulting from two very different microscopic models suggest that the quantum interference effects induced by SOC disorder potentials and the electric field are fairly universal transport phenomena.

V. CURRENT-INDUCED SPIN POLARIZATION AND SPIN CURRENT

In this section, we use the linear response matrix equation, Eq. (16), to discuss the phenomena of current-induced spin polarization and current-induced spin current. Invert the matrix in Eq. (16) and solve for \mathcal{J}_y^z and \mathcal{M}^y as a function of E_x and considering that the spin-charge conversion rates (i.e. $\alpha_{\text{asp}} \tau_{\text{D}}, \theta_{\text{SH}}, \alpha_{\text{R}} \tau_{\text{D}}$) are typically small, we obtain the following results within linear response theory:

$$\mathcal{J}_y^z = (\sigma_{\text{SH}} + \sigma_{\text{ind}}) E_x, \quad \mathcal{M}^y = (\sigma_{\text{DMC}} + \sigma_{\text{EE}}) E_x. \quad (23)$$

These two equations account for the charge-induced spin current and spin polarization, respectively. The ratio of the spin current (spin polarization) to the electric field corresponds to the conversion efficiency of the material.

The current-induced-spin current receives direct and indirect contributions: The direct contribution is proportional to the spin-Hall conductivity σ_{SH} and arises from the SHE, which converts the charge current J_x into the spin-current \mathcal{J}_y^z . An indirect contribution to the spin current is proportional to σ_{ind} and arises in a two-step process in which $J_x \rightarrow \mathcal{M}^y$ – by virtue of ASP scattering – followed by a process in which $\mathcal{M}^y \rightarrow \mathcal{J}_y^z$, by virtue of the precession induced by the Rashba field⁴⁵. The spin conductivities are given by

$$\sigma_{\text{SH}} = -\omega_c \tau_{\text{D}} \sigma_{\text{D}} - v_0 \lambda_z p_F^2 n \tau_{\text{D}} - n \lambda_z \quad (24)$$

$$\sigma_{\text{ind}} = (\alpha_{\text{R}} \tau_{\text{D}})(\alpha_{\text{asp}} \tau_{\text{EY}}^y) \sigma_{\text{D}} \quad (25)$$

Similarly, the current-induced spin polarization also receives direct and indirect contributions. The direct contribution is characterized by the direct-magneto electric coupling σ_{DMC} and it arises from a conversion $J \rightarrow \mathcal{M}$ process. The indirect contribution arises from the Edelstein effect^{5,10} σ_{EE} and it is characterized by the conversion sequence $J_x \rightarrow \mathcal{J}_y^z \rightarrow \mathcal{M}^y$. Their explicit form is given by

$$\sigma_{\text{DMC}} = (\alpha_{\text{asp}} \tau_{\text{s}}^y) \sigma_{\text{D}}, \quad \sigma_{\text{EE}} = (\alpha_{\text{R}} \tau_{\text{s}}^y) \sigma_{\text{SH}}. \quad (26)$$

The total spin relaxation time τ_{s}^y consists of the Elliott-Yafet and D'yakonov-Perel mechanisms:

$$\frac{1}{\tau_{\text{s}}^y} = \frac{1}{\tau_{\text{EY}}^y} + \frac{1}{\tau_{\text{DP}}}. \quad (27)$$

Here $\tau_{\text{DP}}^{-1} = \tau_{\text{D}}(\alpha_{\text{R}}^2 - \alpha_{\text{asp}}^2)$. Note that σ_{DMC} arises from the ASP scattering. We would like to stress that this is different from the microscopic origin of the Edelstein effect⁴⁵, for which the non-equilibrium spin polarization

arises via the conversion sequence: $J_x \rightarrow \mathcal{J}_y^z \rightarrow \mathcal{M}^y$. Note that the figures of merit of current-induced spin polarization, σ_{EE} and σ_{DMC} , are proportional to the total spin relaxation time. In non-uniform systems, ASP modifies the spin continuity equation as follow:

$$[\nabla_t m]^a + [\nabla_i \mathcal{J}_i]^a = -\frac{m^a}{\tau_{\text{EY}}^a} + \alpha_{\text{asp}} \epsilon^{ajz} J_j. \quad (28)$$

which can be derived from the Quantum Boltzmann equation as explained in Ref. 23. Here ϵ^{ijk} is the Levi-Civita antisymmetric tensor. Note that ASP scattering is a form of direct magnetoelectric coupling (DMC) since it couples spin density m^a to the electric current J_i (hence electric field) directly in the spin continuity equation without resorting to any constitutive relations.

VI. DISCUSSIONS OF EXPERIMENTS

The Spin Hall effect (SHE) and the current-induced spin polarization (CISP) are ubiquitous transport phenomena that have been observed in Ref. 46–48 and Ref. 11, 12, 49, and 50, respectively. Although their relative contributions to the overall spin-charge conversion will depend on the microscopic details of the materials, both effects can occur together and couple with each other on symmetry grounds²⁰. In order to differentiate CISP from SHE, Ref. 51 used optical Kerr-rotations to study the direction of the spin polarization and its spatial accumulations. In addition to optical methods, some authors of the present article also proposed an all-electrical experiment²³ in order to differentiate SHE from CISP, based on the theory first developed in Ref. 52.

Recently, J. Bindel *et al.* reported on the fluctuations of Rashba SOC in InSb inversion layer⁴¹. From the Supplementary Material of Ref. 41, the elastic scattering time $\tau_{\text{D}} \sim 200\text{ps}$ and the *giant* uniform Rashba SOC strength $\alpha = 1.2\text{eV}\text{\AA}$. From Fig. 3f of Ref. 41, we can estimate the correlation between fluctuating Rashba strength and the 2D potential energy, $\lambda_{\perp}^2/\xi \sim 12\text{\AA}$. Therefore, $\alpha_{\text{asp}}^{-1} \sim 10^4 \tau_{\text{D}}$, $\tau_{\text{EY}} \sim 10^3 \tau_{\text{D}}$, meaning that we are in the limit $\alpha_{\text{asp}}^{-1} > \tau_{\text{EY}} \gg \tau_{\text{D}}$. In terms of spin-charge conversion efficiencies, we found $\sigma_{\text{DMC}}/\sigma_{\text{EE}} = \alpha_{\text{asp}}/(\alpha_{\text{R}}\theta_{\text{SH}}) \sim 10^{-3}$ due to the large spin Hall angle arising from the giant uniform Rashba SOC, i.e. the spin Hall angle is dominated by intrinsic contribution $\theta_{\text{SH}} \sim \omega_c \tau_{\text{D}} \sim 1$. Hence, the SHE dominates the CISP in Ref. 41.

The ratio $\sigma_{\text{DMC}}/\sigma_{\text{EE}}$ can be enhanced in 2D systems with small or vanishing uniform Rashba SOC like symmetrically doped 2DEG²⁹ or adatoms decorated graphene²⁰. This is because in our theory, the DMC arises from the extrinsic mechanism (i.e. ASP scattering), whereas both SHE and the conversion between spin-current and spin density receive contributions from both extrinsic and intrinsic mechanisms. It is interesting to understand how can DMC occur in 2D systems without relying on disorder potentials that break spatial inversion symmetry.

Note that our calculations are presented for the zero temperature case. At finite temperature, and if the system can support resonant scattering (as in the case of adatoms decorated graphene) finite temperature effects will broaden the line width and decrease the amplitude of the spin Hall conductivity, as described in Ref. 53. We expect the same finite temperature behaviour to occur in σ_{DMC} as well since the broadening of line width and decrease in peak amplitude results from averaging on the number of states near the Fermi surface, and is largely independent of the scattering mechanism. However, in a 2DEG resonant scattering is difficult to observe due to the lack of energy dependence of its density of states. From Eq. 26, $\sigma_{\text{DMC}} = \alpha_{\text{asp}} \tau_s^y \sigma_D$ and Eq. 21 $\alpha_{\text{asp}} = -4\lambda_{xy}\lambda_z\tau_D^{-1}$, we found that the temperature dependence of DMC follows from the temperature dependence of the total spin relaxation time: $\sigma_{\text{DMC}}(T) \propto \tau_s^y(T)$. The temperature dependence of spin relaxation time depends on the microscopic details of a particular system (e.g. mobility, symmetrically or asymmetrically doped quantum well). For example, Ref. 54 reported D'yakonov-Perel mechanism as the dominant spin relaxation channel in their experiment and it has interesting non-monotonic temperature dependence. Therefore, DMC would still be observable at temperature where spin-relaxation time does not vanish.

VII. SUMMARY AND OUTLOOK

In this work we have obtained the linear response of a two-dimensional electron gas under the influence of both intrinsic SOC and a smooth disorder SOC landscape. In particular, by accounting for both spin-conserving (Mott) and spin non-conserving (Rashba) scattering processes, we have found that the quantum interference between them gives rise to the anisotropic spin precession scattering first found in an earlier study of spin-transport in graphene decorated with adatoms²⁰. The anisotropic spin precession scattering is a form of direct magneto electric coupling which gives contributions to both the current-induced spin polarization and the current-induced spin current. Our results suggest that this mechanism, which describes the polarizing effect of the disorder SOC potential should be a rather universal phenomenon in disordered two-dimensional metals lacking inversion symmetry.

ACKNOWLEDGEMENTS

We gratefully acknowledge Roberto Raimondi for kindly delivering a series of lectures on the SU(2)-covariant Schwinger-Keldysh formalism after the workshop ‘‘Recent Progress in Spintronics of 2D Materials’’ held at the National Center for Theoretical Sciences in Taiwan. C.H and M.A.C acknowledge support from the Ministry of Science and Technology (Taiwan) under con-

tract No. NSC 102-2112-M-007-024-MY5 and Taiwan’s National Center of Theoretical Sciences (NCTS). C.H. also acknowledges support from the Singapore National Research Foundation grant No. NRFF2012-02, and from the Singapore Ministry of Education Academic Research Fund Tier 2 Grant No. MOE2015-T2-2-008. M. M. thanks C. Verma for his hospitality at the Bioinformatics Institute in Singapore where this work was initiated. C. H. gratefully acknowledges the hospitality of the Donostia International Physics Center.

Appendix A: Self-energy diagrams and collision integrals

In the Schwinger-Keldysh transport formalism^{55,56}, the collision integral reads

$$I = \int \frac{d\epsilon}{4\pi} (-\Sigma^R G^K - \Sigma^K G^A + G^R \Sigma^K + G^K \Sigma^A), \quad (\text{A1})$$

where G^R, G^A and G^K are the retarded, advanced and Keldysh components of the Green’s function, respectively. Similarly, Σ^R , Σ^A and Σ^K are the retarded, advanced and Keldysh components of the self-energy. The disorder self-energy is a four by four matrix in Keldysh and spin space. In order to evaluate the collision integral, we use the quasi-particle approximation, which approximates

$$G^R(\epsilon, \mathbf{p}) = \frac{1}{\epsilon - \epsilon_p + i\delta}; \quad G^A(\epsilon, \mathbf{p}) = \frac{1}{\epsilon - \epsilon_p - i\delta} \quad (\text{A2})$$

$$G^K(\epsilon, \mathbf{p}) = -2\pi i \delta(\epsilon - \epsilon_p) (1 - 2n_{\mathbf{p}}). \quad (\text{A3})$$

In other words, Eq. (A2) ignores the disorder-induced broadening of the spectral function, whereas Eq. (A3) assumes the existence of a local equilibrium distribution function. The leading order corrections to the collision integral arise from the electric field and are proportional to $E\lambda_{xy}$ and $E\lambda_z$. We will neglect any higher order corrections in the electric field. Since the uniform Rashba SOC is weak and the self-energy is at least second order in the impurity scattering potentials, we will also neglect the correction due to the uniform Rashba SOC potential in the evaluation of the collision integrals, i.e. all collision integrals are zeroth order in the uniform Rashba potential strength α .

Appendix B: Collision integrals

In this appendix, we provide the most important details of the computation of the different contributions to the collision integral, Eq. (11). From here on, we shall use the short-hand notation $p = (\epsilon, \mathbf{p})$, $p' = (\epsilon, \mathbf{p}')$, etc. Note that the energy ϵ is unchanged since scattering with the disorder potential is elastic. The relevant Feynman diagrams are shown in Fig. 2.

1. Drude relaxation: Scalar-scalar self-energy

For this diagram, after disorder average, the Keldysh self-energy matrix is

$$\tilde{\Sigma}(p) = n_i v_0^2 \sum_{\mathbf{p}'} \tilde{G}(p'), \quad (\text{B1})$$

where the tilde means that the (Green's) function is SU(2) locally covariant. After inserting this result into Eq. (A1), the resulting collision integral yields the standard Drude relaxation term:

$$I_D[n_{\mathbf{p}}] = 2\pi n_i v_0^2 \sum_{\mathbf{p}'} (n_{\mathbf{p}'} - n_{\mathbf{p}}) \delta(\epsilon_p - \epsilon_{p'}). \quad (\text{B2})$$

The Drude term drives the relaxation of the charge and spin current.

2. Anisotropic spin precession scattering: Mott-Rashba self-energy

The self-energy for anisotropic spin precession scattering is given by:

$$\begin{aligned} \tilde{\Sigma}(p) = i n_i v_0^2 \lambda_{xy} \lambda_z \sum_{\mathbf{p}'} & \left(\Gamma_M(\mathbf{p}, \mathbf{p}') \tilde{G}(p') \Gamma_R(\mathbf{p} + \mathbf{p}') \right. \\ & \left. - \Gamma_R(\mathbf{p} + \mathbf{p}') \tilde{G}(p') \Gamma_M(\mathbf{p}, \mathbf{p}') \right). \end{aligned} \quad (\text{B3})$$

Notice that it corresponds to a quantum interference process between the Mott and Rashba-type components of the SOC disorder potential. The resulting collision integral can be split as the sum $I_{\text{ASP}} = I_{\text{ASP}}^0[n_{\mathbf{p}}] + I_{\text{ASP}}^1[n_{\mathbf{p}}]$.

$$\begin{aligned} I_{\text{ASP}}^0[n_{\mathbf{p}}] = 2\pi n_i v_0^2 \lambda_{xy} \lambda_z i \sum_{\mathbf{p}'} & \delta(\epsilon_p - \epsilon_{p'}) \\ \times \left(\Gamma_R(\mathbf{p} + \mathbf{p}') n_{\mathbf{p}'} \Gamma_M(\mathbf{p}, \mathbf{p}') - \Gamma_M(\mathbf{p}, \mathbf{p}') n_{\mathbf{p}'} \Gamma_R(\mathbf{p} + \mathbf{p}') \right. \\ \left. + \frac{1}{2} \{ [\Gamma_M(\mathbf{p}, \mathbf{p}'), \Gamma_R(\mathbf{p} + \mathbf{p}')] , n_{\mathbf{p}} \} \right) \end{aligned} \quad (\text{B4})$$

Using the *ansatz* (12) introduced in Sec. IV, we obtain

$$\begin{aligned} \sum_{\mathbf{p}} I_{\text{ASP}}^0[n_{\mathbf{p}}] &= \sum_{\mathbf{p}} I_{\text{ASP}}[\delta(\epsilon_p - \mu) \mathbf{v}_c \cdot \mathbf{p}] \\ &= \frac{4 \lambda_{xy} \lambda_z}{\tau_D v_F} (\sigma^y J_x - \sigma^x J_y) \end{aligned} \quad (\text{B5})$$

The second part of the collision integral resembles a precession term that can be absorbed into the right-hand side of the Boltzmann equation (i.e. the non-dissipative part):

$$I_{\text{ASP}}^1[n_{\mathbf{p}}] = 2\pi^2 i \lambda_z \lambda_{xy} n_i v_0^2 N_0^2 p_F^{-3} \kappa(D, \epsilon_F) [\Gamma_R(\mathbf{p}), n_{\mathbf{p}}]. \quad (\text{B6})$$

Here $\kappa(D, \epsilon_F)$ is a parameter depending on the energy cut-off (bandwidth) D and Fermi energy ϵ_F :

$$\kappa(D, \epsilon_F) = \mathcal{P} \int_0^D \frac{d\epsilon}{\pi} \left[\frac{\epsilon}{\epsilon_F - \epsilon} \right] \quad (\text{B7})$$

3. The \star diagram: Scalar-Rashba self-energy

In this case the self-energy is

$$\begin{aligned} \tilde{\Sigma}(p) = -n_i v_0^2 \lambda_{xy} \sum_{\mathbf{p}'} & \left(\{ \tilde{G}(p'), \Gamma_R(\mathbf{p} + \mathbf{p}') \} \right. \\ & \left. + i e \left[\partial_\epsilon \tilde{G}(p'), (\mathbf{E} \times \boldsymbol{\sigma}) \cdot \mathbf{z} \right] \right) \end{aligned} \quad (\text{B8})$$

The related collision integral is $I[n_{\mathbf{p}}] = I_{\star}^0[n_{\mathbf{p}}] + I_{\star}^1[n_{\mathbf{p}}]$ where

$$I_{\star}^0[n_{\mathbf{p}}] = 2\pi n_i v_0^2 \lambda_{xy} \sum_{\mathbf{p}'} \delta(\epsilon_p - \epsilon_{p}') \{ \Gamma_R(\mathbf{p}' + \mathbf{p}), n_{\mathbf{p}'} - n_{\mathbf{p}} \} \quad (\text{B9})$$

$$\begin{aligned} I_{\star}^1[n_{\mathbf{p}}] = 2\pi n_i v_0^2 \lambda_{xy} \sum_{\mathbf{p}'} & \partial_{\epsilon_p} \delta(\epsilon_p - \epsilon_{p}') \\ \times i [(-e\mathbf{E}) \cdot (\boldsymbol{\sigma} \times \hat{\mathbf{z}}), n_{\mathbf{p}'}]. \end{aligned} \quad (\text{B10})$$

$I_{\star}^1[n]$ is proportional to En_i and it contributes to the anomalous velocity. In the linear response regime, $I_{\star}^1[n_{\mathbf{p}}^0] = 0$ for a spin-unpolarized ground state. Using the drift velocity *ansatz*, $\sum_{\mathbf{p}} I_{\star}^0[\delta n_{\mathbf{p}}] = \sum_{\mathbf{p}} \mathbf{p} I_{\star}^0[\delta n_{\mathbf{p}}] = 0$, since $\Gamma_R \propto \cos \theta$ while $\delta n_{\mathbf{p}'} - \delta n_{\mathbf{p}} \propto \sin \theta$, where $\theta = (\theta_p - \theta_{p'})/2$.

4. Rashba-scattering: Rashba-scalar-scalar self-energy

For this diagram, after disorder average, the self-energy reads:

$$\begin{aligned} \tilde{\Sigma}(p) = -n_i v_0^3 \lambda_{xy} \sum_{\mathbf{p}_a \mathbf{p}_b} & \left[\Gamma_R(\mathbf{p} + \mathbf{p}_a) \tilde{G}(p_a) \tilde{G}(p_b) \right. \\ & \left. + \tilde{G}(p_a) \Gamma_R(\mathbf{p}_a + \mathbf{p}_b) \tilde{G}(p_b) + \tilde{G}(p_a) \tilde{G}(p_b) \Gamma_R(\mathbf{p} + \mathbf{p}_b) \right] \end{aligned} \quad (\text{B11})$$

The resulting collision integral is given by the following expression:

$$I_{\text{RS}}[n_{\mathbf{p}}] = 2\pi^2 n_i v_0^3 \lambda_{xy} p_F^{-1} N_0^2 i [n_{\mathbf{p}}, \Gamma_R(\mathbf{p})] \quad (\text{B12})$$

where $N_0 = \sum_{\mathbf{p}} \delta(\epsilon - \epsilon_p) = m/2\pi$ is the density of states. Together with I_{ASP}^1 , they can be absorbed into the SOC gauge field $\mathcal{A}_y^x = 2m\alpha$ on the right-hand side of the quantum Boltzmann equation and this leads to a renormalization of the parameter $\alpha \rightarrow \alpha + \delta\alpha_R$ where

$$\delta\alpha_R = n_i \pi v_0^2 N_0^2 p_F^{-1} \lambda_{xy} (v_0^2 - \lambda_z \kappa(D, \epsilon_F)). \quad (\text{B13})$$

5. Elliott-Yafet relaxation: Rashba-Rashba and Mott-Mott self-energy

The self-energy leading to spin-relaxation by the Elliott-Yafet mechanism is given by the following expression:

$$\tilde{\Sigma}(p) = n_i v_0^2 \lambda_{xy}^2 \sum_{\mathbf{p}'} \Gamma_R(\mathbf{p} + \mathbf{p}') \tilde{G}(p') \Gamma_R(\mathbf{p} + \mathbf{p}'). \quad (\text{B14})$$

$$\tilde{\Sigma}(p) = -n_i v_0^2 \lambda_z^2 \sum_{\mathbf{p}'} \Gamma_M(\mathbf{p}, \mathbf{p}') \tilde{G}(p') \Gamma_M(\mathbf{p}', \mathbf{p}). \quad (\text{B15})$$

The resulting collision integral is the Elliott-Yafet spin relaxation term coming from the Mott-vertex and the Rashba vertex $I_{\text{EY}}[n_{\mathbf{p}}] = I_{\text{EY}}^M[n_{\mathbf{p}}] + I_{\text{EY}}^R[n_{\mathbf{p}}]$:

$$I_{\text{EY}}^R[n_{\mathbf{p}}] = 2\pi n_i v_0^2 \lambda_{xy}^2 \sum_{\mathbf{p}'} \delta(\epsilon_p - \epsilon_{p'}) \left[\Gamma_R(\mathbf{p} + \mathbf{p}') n_{\mathbf{p}'} \times \Gamma_R(\mathbf{p} + \mathbf{p}') - \frac{1}{2} \{ \Gamma_R^2(\mathbf{p} + \mathbf{p}'), n_{\mathbf{p}'} \} \right]. \quad (\text{B16})$$

$$I_{\text{EY}}^M[n_{\mathbf{p}}] = 2\pi n_i v_0^2 \lambda_z^2 \sum_{\mathbf{p}'} \delta(\epsilon_p - \epsilon_{p'}) \left[\Gamma_M(\mathbf{p}, \mathbf{p}') n_{\mathbf{p}'} \Gamma_M(\mathbf{p}, \mathbf{p}') - \frac{1}{2} \{ \Gamma_M^2(\mathbf{p}, \mathbf{p}'), n_{\mathbf{p}'} \} \right]. \quad (\text{B17})$$

6. Side-jump and swap current: Mott-scalar self-energy

The side-jump self-energy diagram leads to the expression (after disorder average):

$$\tilde{\Sigma}(p) = -\lambda_z n_i v_0^2 \sum_{\mathbf{p}'} i [\Gamma_M(\mathbf{p}, \mathbf{p}'), G(p')] + (-e\mathbf{E}) \partial_{\epsilon} \cdot \frac{1}{2} \left\{ \boldsymbol{\sigma} \times (\mathbf{p} - \mathbf{p}'), \tilde{G}(p') \right\} \quad (\text{B18})$$

The resulting collision integral is given by the sum $I_{\text{SJ}}[n_{\mathbf{p}}] = I_{\text{SJ}}^0[n_{\mathbf{p}}] + I_{\text{SJ}}^1[n_{\mathbf{p}}]$, where

$$I_{\text{SJ}}^1[n_{\mathbf{p}}] = \lambda_z \pi n_i v_0^2 \sum_{\mathbf{p}'} \partial_{\epsilon_p} \delta(\epsilon_p - \epsilon_{p'}) \times \{ (-e\mathbf{E}) \cdot (\boldsymbol{\sigma} \times (\mathbf{p} - \mathbf{p}')), n_{\mathbf{p}} - n_{\mathbf{p}'} \} \quad (\text{B19})$$

$$I_{\text{SJ}}^0[n_{\mathbf{p}}] = 2\pi n_i \lambda_z v_0^2 i \sum_{\mathbf{p}'} \delta(\epsilon_p - \epsilon_{p'}) [n_{\mathbf{p}'}, \Gamma_M(\mathbf{p}, \mathbf{p}')] \quad (\text{B19})$$

7. Skew scattering: Mott-scalar-scalar self-energy

The contribution to self-energy that gives rise to Mott's skew scattering is given by the following expression:

$$\tilde{\Sigma}(p) = -i \lambda_z n_s v_0^3 \sum_{\mathbf{p}_a \mathbf{p}_b} \left(\tilde{G}(p_a) \Gamma_M(\mathbf{p}_a, \mathbf{p}_b) \tilde{G}(p_b) + \tilde{G}(p_a) \tilde{G}(p_b) \Gamma_M(\mathbf{p}_b, \mathbf{p}) + \Gamma_M(\mathbf{p}, \mathbf{p}_a) \tilde{G}(p_a) \tilde{G}(p_b) \right).$$

The resulting collision integral is given by

$$I_{\text{SK}}[n_{\mathbf{p}}] = -2\pi^2 n_s v_0^3 N_0 \lambda_z \sum_{p'} \delta(\epsilon_p - \epsilon_{p'}) \{ \Gamma_M(\mathbf{p}', \mathbf{p}), n_{\mathbf{p}'} \}, \quad (\text{B20})$$

Collecting all the contributions to collision integral from the seven self-energy diagrams, we obtain the complete collision integral used in the main text of the article.

¹ A. Soumyanarayanan, N. Reyren, A. Fert, and C. Panagopoulos, *Nature* **539**, 509 (2016).

² J. Wunderlich, B.-G. Park, A. C. Irvine, L. P. Zárbo, E. Rozkotová, P. Nemeč, V. Novák, J. Sinova, and T. Jungwirth, *Science* **330**, 1801 (2010).

³ J. Sinova, S. O. Valenzuela, J. Wunderlich, C. H. Back, and T. Jungwirth, *Rev. Mod. Phys.* **87**, 1213 (2015).

⁴ Y. Bychkov and E. Rashba, *Sov. Phys. JETP* **39**, 78 (1984).

⁵ V. Edelstein, *Solid State Communications* **73**, 233 (1990).

⁶ J. Sinova, D. Culcer, Q. Niu, N. Sinitsyn, T. Jungwirth, and A. MacDonald, *Phys. Rev. Lett.* **92**, 126603 (2004).

⁷ J. Hirsch, *Phys. Rev. Lett.* **83**, 1834 (1999).

⁸ N. Nagaosa, J. Sinova, S. Onoda, A. H. MacDonald, and N. P. Ong, *Rev. Mod. Phys.* **82**, 1539 (2010).

⁹ S. Zhang and A. Fert, *Phys. Rev. B* **94**, 184423 (2016).

¹⁰ A. Maleki, R. Raimondi, and K. Shen, arXiv:1610.08258v1 (2016).

¹¹ Q. Song, J. Mi, D. Zhao, T. Su, W. Yuan, W. Xing, Y. Chen, T. Wang, T. Wu, X. H. Chen, *et al.*, *Nature Communications* **7** (2016).

¹² Q. Song, H. Zhang, T. Su, W. Yuan, Y. Chen, W. Xing, J. Shi, J. Sun, and W. Han, *Science Advances* **3**, e1602312 (2017).

¹³ C. Gorini, A. Maleki, K. Shen, I. Tokatly, G. Vignale, and R. Raimondi, arXiv:1702.04887v1 (2017).

¹⁴ E. G. Mishchenko, A. V. Shytov, and B. I. Halperin, *Phys. Rev. Lett.* **93**, 226602 (2004).

¹⁵ S. D. Ganichev, M. Trushin, and J. Schliemann, arXiv:1606.02043 (2016).

- ¹⁶ R. R. A. F. Manuel Offidani, Mirco Milletar, arXiv:1706.08973 (2017).
- ¹⁷ A. H. Castro Neto and F. Guinea, Phys. Rev. Lett. **103**, 026804 (2009).
- ¹⁸ C. Weeks, J. Hu, J. Alicea, M. Franz, and R. Wu, Phys. Rev. X **1**, 021001 (2011).
- ¹⁹ A. Ferreira, T. G. Rappoport, M. A. Cazalilla, and A. C. Neto, Phys. Rev. Lett. **112**, 066601 (2014).
- ²⁰ C. Huang, Y. D. Chong, and M. A. Cazalilla, Phys. Rev. B **94**, 085414 (2016).
- ²¹ M. Milletari and A. Ferreira, Phys. Rev. B **94**, 201402 (2016).
- ²² M. Milletari and A. Ferreira, Phys. Rev. B **94**, 134202 (2016).
- ²³ C. Huang, Y. Chong, and M. Cazalilla, arXiv:1702.04955 (2017).
- ²⁴ F. S. Bergeret and I. V. Tokatly, Phys. Rev. B **94**, 180502 (2016).
- ²⁵ a. Ilya Tokatly, (2017).
- ²⁶ A. Zyuzin, M. Alidoust, and D. Loss, Phys. Rev. B **93**, 214502 (2016).
- ²⁷ I. V. Bobkova, A. M. Bobkov, A. A. Zyuzin, and M. Alidoust, Phys. Rev. B **94**, 134506 (2016).
- ²⁸ J. Balakrishnan, G. K. W. Koon, M. Jaiswal, A. H. C. Neto, and B. Özyilmaz, Nature Physics **9**, 284 (2013).
- ²⁹ M. Glazov, E. Y. Sherman, and V. Dugaev, Physica E: Low-dimensional Systems and Nanostructures **42**, 2157 (2010).
- ³⁰ Z. Wang, D.-K. Ki, J. Y. Khoo, D. Mauro, H. Berger, L. S. Levitov, and A. F. Morpurgo, Phys. Rev. X **6**, 041020 (2016).
- ³¹ B. Yang, M.-F. Tu, J. Kim, Y. Wu, H. Wang, J. Alicea, M. Bockrath, and J. Shi, 2D Mater. **3**, 031012 (2016).
- ³² A. H. Castro Neto, F. Guinea, N. Peres, K. S. Novoselov, and A. K. Geim, Rev. Mod. Phys. **81**, 109 (2009).
- ³³ S. Das Sarma, S. Adam, E. H. Hwang, and E. Rossi, Rev. Mod. Phys. **83**, 407 (2011).
- ³⁴ D. C. Tsui, H. L. Stormer, and A. C. Gossard, Phys. Rev. Lett. **48**, 1559 (1982).
- ³⁵ E. Y. Sherman, Applied Physics Letters **82**, 209 (2003).
- ³⁶ S. A. Tarasenko, Phys. Rev. B **73**, 115317 (2006).
- ³⁷ S. A. Tarasenko, JETP Letters **84**, 199 (2006).
- ³⁸ K. Shen, R. Raimondi, and G. Vignale, Phys. Rev. B **90**, 245302 (2014).
- ³⁹ R. Raimondi, P. Schwab, C. Gorini, and G. Vignale, Annalen der Physik **524**, n/a (2012).
- ⁴⁰ R. Raimondi, C. Gorini, P. Schwab, and M. Dzierzawa, Phys. Rev. B **74**, 035340 (2006).
- ⁴¹ J. R. Bindel, M. Pezzotta, J. Ulrich, M. Liebmann, E. Y. Sherman, and M. Morgenstern, Nature Physics **12**, 920 (2016).
- ⁴² J. M. Luttinger and W. Kohn, Phys. Rev. **109**, 1892 (1958).
- ⁴³ C. Huang, Y. D. Chong, G. Vignale, and M. A. Cazalilla, Phys. Rev. B **93**, 165429 (2016).
- ⁴⁴ L. D. Landau and E. M. Lifshitz, *Statistical Physics, Part I, Volume 5 of Course of Theoretical Physics* (Pergamon, 1980).
- ⁴⁵ K. Shen, G. Vignale, and R. Raimondi, Phys. Rev. Lett. **112**, 096601 (2014).
- ⁴⁶ Y. Kato, R. Myers, A. Gossard, and D. Awschalom, science **306**, 1910 (2004).
- ⁴⁷ S. Valenzuela and M. Tinkham, Nature **442**, 176 (2006).
- ⁴⁸ A. Avsar, J. H. Lee, G. K. W. Koon, and B. Özyilmaz, 2D Materials **2**, 044009 (2015).
- ⁴⁹ J. R. Sánchez, L. Vila, G. Desfonds, S. Gambarelli, J. Attané, J. De Teresa, C. Magén, and A. Fert, Nature communications **4** (2013).
- ⁵⁰ Y. K. Kato, R. C. Myers, A. C. Gossard, and D. D. Awschalom, Phys. Rev. Lett. **93**, 176601 (2004).
- ⁵¹ V. Sih, R. Myers, Y. Kato, W. Lau, A. Gossard, and D. Awschalom, Nature Physics **1**, 31 (2005).
- ⁵² D. A. Abanin, A. V. Shytov, L. S. Levitov, and B. I. Halperin, Phys. Rev. B **79**, 035304 (2009).
- ⁵³ H.-Y. Yang, C. Huang, H. Ochoa, and M. A. Cazalilla, Phys. Rev. B **93**, 085418 (2016).
- ⁵⁴ L. Han, Y. Zhu, X. Zhang, P. Tan, H. Ni, and Z. Niu, Nanoscale research letters **6**, 84 (2011).
- ⁵⁵ J. Rammer and H. Smith, Rev. Mod. Phys. **58**, 323 (1986).
- ⁵⁶ J. Rammer, *Quantum Field Theory of Non-equilibrium States* (Cambridge University Press, 2011).